Acigöl rhyolite field, central Anatolia (part II): geochemical and isotopic (Sr–Nd–Pb, $\delta^{18}O$) constraints on volcanism involving two high-silica rhyolite suites

W. Siebel, A. K. Schmitt, E. Kiemele, M. Danišík & F. Aydin

Contributions to Mineralogy and Petrology

ISSN 0010-7999
Volume 162
Number 6

Contrib Mineral Petrol (2011)
162:1233-1247
DOI 10.1007/s00410-011-0651-2

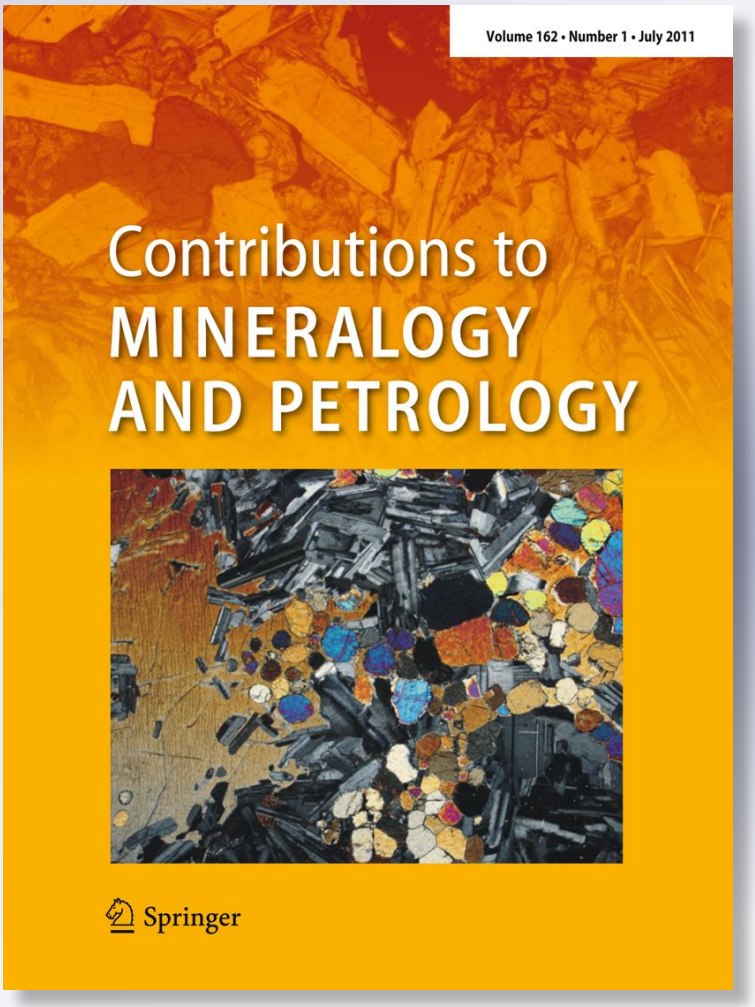

Springer

Contrib Mineral Petrol (2011) 162:1233–1247
DOI 10.1007/s00410-011-0651-2

ORIGINAL PAPER

Acigöl rhyolite field, central Anatolia (part II): geochemical and isotopic (Sr–Nd–Pb, $\delta^{18}O$) constraints on volcanism involving two high-silica rhyolite suites

W. Siebel · A. K. Schmitt · E. Kiemele · M. Danišík · F. Aydin

Received: 22 January 2011 / Accepted: 7 May 2011 / Published online: 7 June 2011

Abstract The Acigöl rhyolite field erupted the most recent high-silica rhyolites within the Cappadocian Volcanic Province of central Anatolia, Turkey. It comprises two sequences of domes and pyroclastic rocks with eruption ages of ~150–200 ka (eastern group) and ~20–25 ka (western group). Compositionally, the eastern rhyolite group lavas are less evolved (SiO_2 = 74–76 wt%), whereas the western group has higher silica abundance (SiO_2 = ~77 wt%) with extremely depleted feldspar-compatible trace elements. Within each group, compositional variability is small and $^{143}Nd/^{144}Nd$ (0.51257–0.51265) and Pb isotope compositions ($^{206}Pb/^{204}Pb$ = 18.87–18.88, $^{207}Pb/^{204}Pb$ = 15.65–15.67 and $^{208}Pb/^{204}Pb$ = 38.94–38.98) are homogeneous. The western group rhyolites have $\delta^{18}O$(zircon) overlapping mantle values (5.7 ± 0.2‰), whereas eastern group rhyolites are enriched in $\delta^{18}O$ by ~0.5‰, consistent with a tendency to lower εNd values. By contrast, western group rhyolites have markedly more radiogenic $^{87}Sr/^{86}Sr$ ratios (0.7065–0.7091) compared to those of the eastern group (0.7059–0.7065). The presence of angular granitic xenoliths and a correlation between hydration (based on loss on ignition data) and $^{87}Sr/^{86}Sr$ in the western lavas, however, indicates that Sr was added during the eruption or post-eruption alteration. Isotope constraints preclude the possibility that the rhyolite magmas formed by partial melting of any known regional crystalline basement rocks. Basalts and andesites erupted in the periphery of the Acigöl field are characterised by $^{87}Sr/^{86}Sr$ ratios between 0.7040 and 0.7053, $^{143}Nd/^{144}Nd$ = 0.51259–0.51300, $^{206}Pb/^{204}Pb$ = 18.85–18.87, $^{207}Pb/^{204}Pb$ = 15.646–15.655, $^{208}Pb/^{204}Pb$ = 38.90–38.97. The isotopic and trace element data favour an origin of the rhyolites by mixing of basaltic/andesitic magmas with minor amounts of crustal melts and followed by extensive fractional crystallization.

Keywords Acigöl · $\delta^{18}O$ in zircon · Rhyolite · Silicic volcanism · Sr–Nd–Pb isotopes

Communicated by J. Hoefs.

W. Siebel (✉) · E. Kiemele
Department of Geosciences, University of Tübingen, Tübingen, Germany
e-mail: wolfgang.siebel@uni-tuebingen.de

A. K. Schmitt
Department of Earth and Space Sciences, University of California, Los Angeles, CA, USA

M. Danišík
Department of Earth and Oceanic Sciences, University of Waikato, Hamilton, New Zealand

M. Danišík
John de Laeter Centre for Isotope Research, Applied Geology, Curtin University, Perth, Australia

F. Aydin
Department of Geological Engineering, Karadeniz Technical University, Trabzon, Turkey

Introduction

Catastrophic caldera-forming rhyolite eruptions provide important stratigraphic markers, and the largest eruptions have global impacts (Rampino and Self 1992; Jones 2007; Saunders et al. 2010). At the other end of the volumetric spectrum of rhyolite volcanism, there are clusters and chains of lava domes. These are individually small in volume, but collectively long-lived and capable of producing sizeable accumulations of rhyolite (e.g. Christiansen 2001). Small-volume rhyolite eruptions are frequently

interpreted as harbingers of much larger magma volumes at depth and rhyolite fields thus may be, but are not necessarily precursors to supervolcanic eruptions (Metz and Mahood 1985). To better constrain the extrusive to intrusive volume relationships for rhyolites, extensive fractionation needs to be accounted for that produces the low abundances of feldspar-compatible trace elements such as Sr, Ba and Eu that are characteristic for many high-silica (>75 wt% SiO_2) suites. Fractionation could conceivably occur in mostly crystalline mushes of intermediate bulk composition, whereby interstitial residual melts are extracted to form aphyric rhyolites (Bachmann and Bergantz 2004; Glazner et al. 2008). Alternatively, high-silica rhyolites can be generated by re-melting of mafic to intermediate rocks (Streck and Grunder 2008), but this requires protracted crystallization given that strong feldspar-compatible element depletion is inconsistent with partial melting of most crustal rocks (Mahood and Halliday 1988; Metz and Mahood 1991). Long-lived rhyolite fields are ideal targets for studying the relationships between high-silica rhyolites and mantle or crustal sources and also for testing models of rhyolite extraction from partially molten mush zones because sequential eruptions often record temporal trends in magma compositions. Isotopic and geochemical fingerprinting can reveal genetic relationships between compositionally variable volcanic rocks. But for high-silica rhyolites, data need to be scrutinised because of the strong leverage that minor amounts of contamination or accessory mineral fractionation can have on strongly depleted trace elements (Miller and Mittlefehldt 1984; Mahood and Halliday 1988).

In this paper, we use major, trace element, and isotope data to explore potential genetic relationships between two phases of silicic volcanism within the Pleistocene Acigöl rhyolite field within the Cappadocian Volcanic Province (CVP) of central Anatolia (Turkey). Although the Acigöl field is dominated by high-silica extrusive rocks and pyroclastic deposits, coeval basaltic eruptions occurred within the marginal regions of the field, resulting in a compositional bimodal suite. In an accompanying study (Schmitt et al. this issue), we have outlined the chronology of the Quaternary Acigöl field based on combined U–Th and (U–Th)/He zircon dating and identified two separate phases of silicic volcanic activity during the Middle and Late Pleistocene with spatially segregated eruption centres in the eastern and western parts of Acigöl, respectively. Geochemical data presented here suggest that the Acigöl rhyolite sequence is not strictly cogenetic. Robust isotopic tracers (Nd whole-rock isotopes, oxygen-in-zircon) support a model of formation by partial melting of hybrid (mantle-dominated) sources and subsequent low-pressure differentiation involving processes of crystal fractionation. The presence of undegassed zircon xenocrysts in the rhyolite, systematic variations of Sr isotopic composition as well as measures for rock hydration imply that the contribution of crustal material will be overestimated if based only on non-robust indicators.

Geological setting

General geology

Central Anatolia, including the CVP, has been subjected to complex tectonic deformations and intensive volcanism since the Late Miocene (Beekman 1966; Innocenti et al. 1975; Pasquarè et al. 1988; Göncüoğlu and Toprak 1992; Temel et al. 1998). Neotectonic features of this region were shaped as a result of convergence between northward-moving African–Arabian and the relatively stable Eurasian plates (Dewey et al. 1986; Dirik and Göncüoğlu 1996; Bozkurt 2001; Şengör et al. 2008). In response to the indentation of the Arabian promontory, central Anatolia is being extruded westwards at rates of 20 mm/year (geodetic monitoring data; Jiménez-Munt et al. 2003; Serpelloni et al. 2007) and convergence and crustal extrusion has led to the development of numerous large-scale faults and uplift of the Anatolian plateau (Pasquarè et al. 1988; Toprak 1998). Central Anatolia is also situated in the back arc of the Cyprus arc-trench system that was intermittently activated during the Early Miocene (Robertson 2000; Stephenson et al. 2004). A northward dipping detached slab is currently imaged beneath eastern Anatolia (Faccenna et al. 2006). In this rather complex tectonic setting, the Neogene volcanism of central Anatolia is illustrative of the transition from continental arc to post-arc magmatism similar to the evolution of other convergent margins (Cousens et al. 2011).

Central Anatolian volcanic activity has produced numerous monogenetic centres, Late Miocene/Early Pliocene (Melendiz Dagi, Keciboyduran Dagi) and Quaternary (Erciyes Dagi, Hasan Dagi) stratovolcanoes and extensive ignimbrite fields (Innocenti et al. 1975; Pasquarè et al. 1988; Le Pennec et al. 1994; Temel et al. 1998; Viereck-Götte et al. 2010). The volcanic rocks cap the Central Anatolian Crystalline Complex (CACC), a basement sequence consisting of Precambrian, Palaeozoic and Mesozoic metamorphic massifs, Cretaceous supra-subduction zone ophiolitic rocks and Cretaceous granitoids (Göncüoğlu 1986; Köksal and Göncüoğlu 2008; Dilek and Sandvol 2009). Volcanic products range widely in composition from basalt to rhyolite and include mainly calc-alkaline andesitic rocks with minor alkali-rich varieties (Deniel et al. 1998; Aydin 2008). Geochemical parameters and the change from calc-alkaline towards more alkaline composition point to the cessation of volatile flux driven

melting in a supra-subduction mantle and a gradually increasing impact of decompression melting of asthenospheric mantle with an intraplate signature (Deniel et al. 1998; Alıcı-Şen et al. 2004).

Silicic volcanism has been extensive in the CVP between the cities of Nevşehir, Niğde and Kayseri. Regionally distributed Neogene ignimbrites erupted from largely hidden calderas reach eruptive volumes of >80 km^3 (dense rock equivalent) (Le Pennec et al. 1994). Erosional remnants of these ignimbrite sheets form a surrealistic landscape that has mesmerized travellers for centuries and bears witness to human settlement since Neolithic times (England et al. 2008; Slimak et al. 2008). In western Cappadocia, Quaternary volcanism is characterised by the preponderance of monogenetic centres (Notsu et al. 1995; Toprak 1998), represented by numerous maars, domes and cinder cones as well as related lava flows of basaltic and rhyolitic composition (Le Pennec et al. 1994). The area is separated by the Erdaş Dagi Miocene–Pliocene volcanic massif (Kürkçüoglu et al. 1998) into the southern 1.7–0.4 Ma old Göllüdag complex and the northern 0.2–0.02 Ma Acigöl complex (Bigazzi et al. 1993; Druitt et al. 1995; Mouralis et al. 2002; Türkecan et al. 2004; Slimak et al. 2008). Tectonic setting of this region is dominated by sinistral shear associated with N–S compression (Druitt et al. 1995; Koçyiğit and Beyhan 1998), and the overall transcurrent fault systems present in central Anatolia provide evidence that the volcanism and caldera formation took place in a locally extensional environment (Pasquarè et al. 1988; Toprak 1998).

Acigöl volcanic complex

The Acigöl volcanic complex (Fig. 1) is a major late Quaternary bimodal centre within the CVP, located approximately between the towns of Acigöl and the western outskirts of Nevşehir. It comprises a rhyolite field consisting of lava domes with associated tuff rings, as well as an apron of air fall and pyroclastic flow deposits, peripheral mafic cones and lava flows. Collectively, the complex covers an area of ~150 km^2 (Batum 1978; Yildirim and Özgür 1981; Druitt et al. 1995; Mouralis et al. 2002; Türkecan et al. 2004). Paroxysmal silicic eruptions resulted in the formation of collapse structures in the eastern part of the complex (Druitt et al. 1995). Deposits from these eruptions comprise two dominantly Plinian-type tephra falls termed Lower Acigöl tuff (LAT; >13 km^3 actual volume, also termed Kumtepe tuff in the older literature; Pasquarè 1968) and Upper Acigöl tuff (UAT; ~15 km^3). Rhyolite and obsidian flows in the eastern part of Acigöl (Bogazköy, Kocadag, Taşkesik) predate the eruption of the Upper Acigöl tuff (Druitt et al. 1995; Schmitt et al. this volume). These Middle Pleistocene lavas and pyroclastic rocks (elsewhere defined as Acigöl-East ante-caldera group; Chataigner et al. 1998) are hereafter referred as the eastern group. A Late Pleistocene rhyolite dome cluster is situated ~5 km west of the older dome complex, and comprises, from north to south, the domes of Karniyarik, Kuzey, Tepeköy, Kaleci, Güneydag and Korudag. The youngest rhyolitic eruption produced a maar

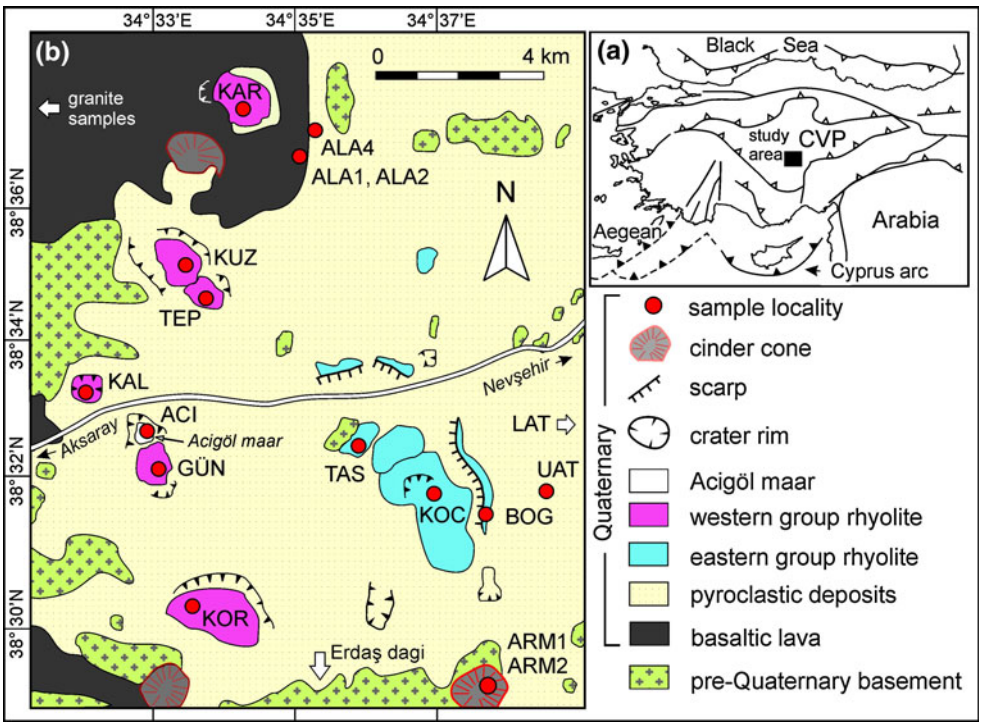

Fig. 1 **a** Location of the Cappadocian Volcanic Province (CVP) in Turkey and **b** sketch map of the study area (redrawn from Druitt et al. 1995) showing geological features of the Acigöl volcanic field, CVP and selected sample sites. *ACI* Acigöl, *ALA* Alacaşar, *ARM* Armutlu tepe, *BOG* Bogazköy, *GÜN* Güneydag, *KAL* Kaleci, *KAR* Karniyarik, *KOC* Kocadag, *KOR* Korudag, *KUZ* Kuzey, *LAT* lower Acigöl tuff, *Tas* Taşkesik, *TEP* Tepeköy, *UAT* upper Acigöl tuff. Sample localities for Lower Acigöl tuff (LAT) and two granites from a basement complex are located outside the map boundary

located on the northern side of Güneydag dome. Combined U–Th and (U–Th)/He zircon chronostratigraphy (Schmitt et al. this volume) supersedes previous subdivisions of the Acigöl rhyolite volcanism that was based on fission track data and field observations (Bigazzi et al. 1993; Druitt et al. 1995). Our new age data show that the volcanic rocks formed during two eruption periods: ~200–150 ka (eastern group) and ~25–20 ka (western group).

The Acigöl rhyolite field is bordered by Quaternary basaltic and andesitic lava flows and scoria cones. The basaltic lavas probably erupted from fissure vents and are primarily distributed around the western and northern periphery of the complex. K/Ar ages for basaltic cones and lava flows adjoining the Acigöl domes range from 154 ± 4 to 34 ± 3 ka (Olanca 1994; Türkecan et al. 2004; Slimak et al. 2008). Altogether, silicic and mafic eruptions form a bimodal magma suite, which has been attributed to partial fusion of the crust and input of melts from the mantle (Druitt et al. 1995). The disproportionate preponderance of felsic lavas and pyroclastic deposits over basalts was explained by a low-density, partial melt zone that prohibits basalts from rising into the rhyolite field (Druitt et al. 1995).

Analytical techniques

Seventeen samples (each 5–7 kg, comprising nine rhyolites, three composite pumices and five basaltic rocks) were analysed for geochemical (major and trace elements) and isotopic (Sr–Nd–Pb) composition. Eastern and western group rhyolites and one obsidian ejecta clast from the wall of Acigöl maar were also selected for δ^{18}O(zircon) isotope analysis. Additionally, two granites sampled close to the Acigöl field were analysed for Sr–Nd–Pb isotopic composition as potential crustal source rocks. All samples were collected in situ from fresh rock exposures. After rinsing and air-drying, they were crushed in a jaw crusher and powdered in an agate mill. Major and trace element compositions were determined by wavelength X-ray fluorescence (XRF) spectrometry on a Bruker AXS S4 pioneer spectrometer, at the University of Tübingen. Loss on ignition (LOI) was calculated after heating the sample powder to 1,050°C for 1 h. Major elements and most trace elements were measured on fused glass beads made from whole rock powder (1.50 g) mixed with 7.50 g of Spectromelt fluxing agent and fused at 1,150°C, whereas other trace elements (Sc, Cu, Ga, Sn, Pb, Cs, Gd, Lu, Cl, F) were determined on pressed powder pellets. Analytical uncertainties range from 1–5% and 5–10% for major and trace elements, respectively, depending on the concentration level.

U and Th concentrations for the silicic rocks were determined by isotope dilution thermal ionisation mass spectrometry (ID-TIMS). Spike solutions containing the enriched tracers of ^{235}U and ^{230}Th were added to the samples prior to dissolution, and U and Th were separated and purified from other major and trace elements by anion chromatography on Bio-Rad AG1X8 anion exchange resin, following the procedures of Goldstein et al. (1989). Both elements were loaded on Re filaments and measured in double-filament mode on a Finnigan MAT 262 multicollector mass spectrometer at the University of Tübingen.

For isotope analyses, approximately 50 mg of whole-rock powder was decomposed in a mixture of HF-$HClO_4$ in Teflon beakers in steel jacket bombs at 180°C for 6 days to ensure total decomposition of refractory phases. Sr and Nd were separated by conventional ion exchange techniques and their isotopic compositions were measured on single W and double Re filament configurations, respectively. The isotopic ratios were corrected for mass fractionation by normalising to ^{86}Sr/^{88}Sr = 0.1194 and ^{146}Nd/^{144}Nd = 0.7219. The reproducibility of ^{87}Sr/^{86}Sr and ^{143}Nd/^{144}Nd during the period of measurement was checked by analyses of NBS 987 Sr and La Jolla Nd standards yielding average values of 0.710235 ± 0.000015 (2SD, $n = 5$) and 0.511840 ± 0.000012 (2SD, $n = 5$), respectively. From this, we estimate a ± 0.4 uncertainty of individual εNd values $(=[(^{143}Nd/^{144}Nd_{sample})/(^{143}Nd/^{144}Nd_{chondrite})-1] \times 10^4)$. Total procedural blanks were <200 pg for Sr and <50 pg for Nd.

Separation and purification of Pb were carried out on Teflon columns with a 100-µl (separation) and 40-µl bed (cleaning) of Bio-Rad AG1-X8 (100–200 mesh) anion exchange resin using a HBr-HCl ion exchange procedure. Pb was loaded with silica gel and phosphoric acid onto a Re filament and was analysed at ~1,300°C in single-filament mode. A factor of 1‰ per atomic mass unit for instrumental mass fractionation was applied to the Pb analyses, using NBS SRM 981 as reference material. Total procedural blanks for Pb during the measurement period were between 15 and 30 pg. Sample reproducibility is estimated at ±0.02, ±0.015 and ±0.03 (2σ) for ^{206}Pb/^{204}Pb ^{207}Pb/^{204}Pb and ^{208}Pb/^{204}Pb ratios, respectively. All isotope compositions (including Sr and Nd) were measured on the Finnigan MAT 262 multicollector mass spectrometer.

Oxygen isotope ratios were determined on the CAMECA ims 1270 high-resolution ion microprobe at UCLA using multi-collection analysis described in Trail et al. (2007). ^{18}O/^{16}O ratios are expressed as δ^{18}O relative to VSMOW standard: $[(^{18}O/^{16}O)_{sample}/(^{18}O/^{16}O)_{VSMOW}-1] \times 10^3$. Instrumental mass fractionation was determined on standard AS3 with $\delta^{18}O_{VSMOW} = 5.34‰$ (Trail et al. 2007). Accuracy was confirmed by replicate analysis of secondary zircon standards 91500 and Pacoima during the same analytical session, which yielded average values of 9.8 ± 0.6‰ (2 SD; $n = 15$) and 5.7 ± 0.8‰; 2 SD;

$n = 15$), respectively. Based on the average external reproducibility of AS3 and secondary standards, we assign a 0.6‰ uncertainty (2σ) to individual zircon $\delta^{18}O$ values.

Rock description

Texturally and compositionally, four major rock types are present in the Acigöl volcanic complex:

(1) Rhyolite lavas of the eastern group (Bogazköy, Taşkesik, Kocadag) display a glassy dark matrix with cryptocrystalline minerals, mainly plagioclase, minor hornblende and biotite. These lavas host some Anatolian sources of vitreous obsidian and perlite used during prehistoric periods (Chataigner et al. 1998; Poupeau et al. 2010). Lavas from Bogazköy and Taşkesik (Fig. 2a) are glassy with small irregular and randomly distributed cavities and spherulitic devitrification (snow-flake obsidian). By contrast, Kocadag rhyolite is completely devitrified has larger microphenocrysts and more abundant quartz.

(2) The rhyolite lavas of the western group are holohyaline with cryptocrystalline plagioclase, quartz, biotite and hornblende. Lavas are vesicular and flow-banded (Fig. 2b). Small (<0.5 mm) holocrystalline, angular xenoliths of altered granite are present (Fig. 2c).

(3) LAT and UAT fibrous pumice are almost entirely holohyaline and indistinguishable in thin section. Pumice clasts are angular and unwelded. All of the rhyolite and pumice samples contain accessory zircon and apatite.

(4) Basaltic lava samples exhibit a seriate texture and contain subhedral phenocrysts of clinopyroxene (Fig. 2d), plagioclase, olivine and hornblende, which are commonly embedded in a cryptocrystalline mafic matrix.

Major and trace element composition

Chemical data and discussions of the geochemical characteristics of the Acigöl silicic rocks can be found in Druitt et al. (1995), Türkecan et al. (2004) and Tryon et al. (2009). Here, we focus mainly on the comparison between eastern and western rhyolites and their relationship to the peripheral basaltic rocks. Representative whole-rock geochemical

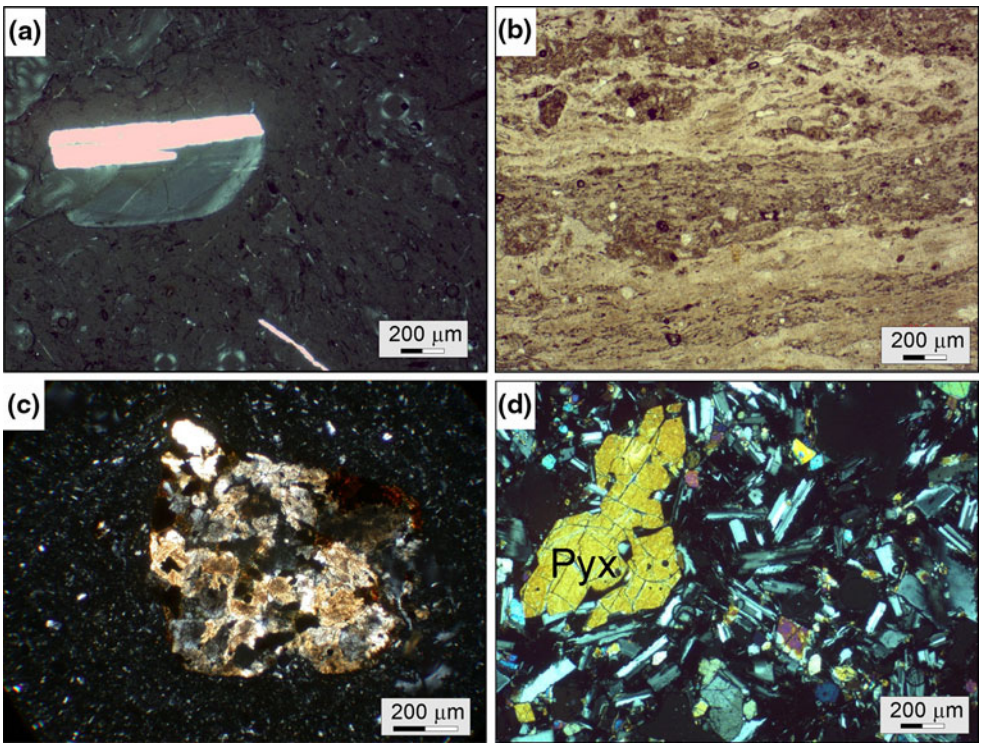

Fig. 2 Thin section photomicrographs from Acigöl volcanic rocks; **a** obsidian from Bogazköy (sample BOG-1) with glassy matrix and embedded hypidiomorphic zoned plagioclase, crossed polarised light; **b** rhyolite from Karniyarik dome (sample KAR-1) under plane polarised light. Cryptocrystalline matrix shows flow-banding. White small structures are spherulites (identified under crossed polarisers); **c** granite xenolith, >500 µm in diameter, in rhyolite lava from Karniyarik dome (sample KAR-1), crossed polarised light; **d** seriate-textured tholeiitic basalt from Alacaşar (sample ALA-1) under crossed polarised light. Deeply embayed subhedral phenocryst of pyroxene surrounded by smaller plagioclase and pyroxene crystals, embedded in a cryptocrystalline mafic matrix

Table 1 Chemical analysis of rock samples from the Acigöl volcanic field

Sample rock type	KAR-2 basalt	ALA-1 basalt	ALA-2 basalt	ARM-1 andesite	ARM-2 andesite	KOC rhyol (I)	ALA-4 pumice (I)	TAS rhyol (I)	BOG-1 rhyol (I)	LAT pumice (I)	UAT pumice (I)	KAL rhyol (II)	TEP rhyol (II)	GÜN rhyol (II)	KUZ rhyol (II)	KOR rhyol (II)	KAR-1 rhyol (II)
SiO_2	51.86	51.91	52.09	58.21	60.23	73.61	74.60	74.68	75.43	75.54	75.61	76.74	76.79	76.79	76.84	76.88	77.05
TiO_2	1.31	1.22	1.25	1.27	0.72	0.13	0.10	0.10	0.09	0.09	0.09	0.04	0.04	0.04	0.04	0.04	0.04
Al_2O_3	16.70	17.08	16.98	17.44	17.13	14.20	13.83	13.87	13.62	13.47	13.50	12.85	12.89	12.94	12.82	12.79	12.73
Fe_2O_3	8.90	8.60	8.57	7.63	6.15	1.91	1.34	1.49	1.18	1.23	1.15	1.01	0.98	0.95	1.01	0.98	1.04
MnO	0.14	0.14	0.14	0.13	0.12	0.06	0.06	0.06	0.06	0.06	0.06	0.07	0.07	0.07	0.07	0.07	0.07
MgO	6.76	7.02	6.99	2.44	3.03	0.19	0.18	0.19	0.14	0.18	0.16	0.09	0.09	0.09	0.08	0.08	0.11
CaO	9.06	9.05	8.94	5.46	6.34	1.09	0.87	0.89	0.78	0.79	0.82	0.42	0.42	0.38	0.41	0.39	0.43
Na_2O	3.81	3.69	3.68	4.82	3.68	4.51	4.23	4.25	4.11	4.00	3.74	4.26	4.27	4.32	4.33	4.33	4.22
K_2O	1.16	1.10	1.15	2.04	2.41	4.25	4.76	4.44	4.55	4.61	4.84	4.49	4.43	4.39	4.38	4.42	4.28
P_2O_5	0.30	0.19	0.20	0.55	0.20	0.04	0.03	0.03	0.02	0.02	0.02	0.02	0.02	0.02	0.02	0.01	0.02
LOI	0.04	0.48	0.48	0.24	0.18	0.29	3.12	2.94	3.10	3.85	3.46	2.11	2.02	2.56	2.26	2.34	3.12
Ba	252	240	253	499	724	459	397	398	334	320	337	8	17	525	24	18	21
Cr	146	163	161	10	31	64	b.d.	50	1	69	3	b.d.	3	b.d.	38	7	37
Ni	128	160	156	56	82	58	56	71	52	70	44	7	25	41	43	30	62
Rb	25	24	26	56	69	148	148	167	174	174	172	257	247	261	242	257	241
Sr	356	358	353	426	432	103	69	76	62	70	71	2	4	20	1	3	7
V	162	158	162	107	139	5	4	8	5	8	3	6	4	6	6	7	7
Y	28	25	26	34	24	22	15	19	19	17	14	31	26	29	27	29	27
Zn	44	49	43	56	33	9	b.d.	18	6	9	9	100	1	3	b.d.	3	16
Zr	152	141	147	253	171	174	119	145	112	107	110	89	86	88	88	88	90
Ce	89	83	b.d.	122	125	82	103	82	72	73	70	77	64	59	63	66	63
Eu	1.2	1.0	1.0	1.7	1.5	0.7	0.1	0.5	0.3	0.6	0.3	0.1	0.3	0.3	0.1	b.d.	0.1
La	10	9	12	32	34	31	27	34	24	29	24	12	11	8	19	14	12
Nb	b.d.	b.d.	b.d.	15	b.d.	16	13	17	16	14	15	30	30	31	28	30	27
Nd	14	6	11	32	22	19	15	13	12	15	25	10	3	5	12	14	13
Sm	2.4	5.9	5.9	8.0	5.2	6.4	b.d.	5.0	3.9	6.4	2.5	3.0	6.3	6.2	3.9	b.d.	3.8
Yb	2.6	2.3	2.4	3.3	2.4	3.2	2.6	3.0	3.1	2.9	2.5	5.2	4.6	5.0	4.7	4.9	4.6
Sc	26	22	24	13	13	2	b.d.	2	b.d.	b.d.	1	3	4	2	b.d.	4	1
Cu	73	70	90	39	46	22	b.d.	26	30	19	13	26	29	26	26	30	15
Ga	38	39	39	44	39	38	b.d.	36	36	36	36	37	37	37	37	37	36
Sn	1	2	2	2	2	2	b.d.	2	2	2	2	3	3	4	3	3	2
Pb	5	5	4	12	25	25	b.d.	24	24	26	24	29	28	28	28	28	22
Cs	b.d.	b.d.	1	b.d.	3	6	b.d.	7	12	7	7	15	17	21	16	23	6
Gd	b.d.	b.d.	b.d.	2	1	5	b.d.	6	7	5	4	7	7	6	7	7	4
Lu	1.1	1.0	1.2	1.2	0.7	0.5	b.d.	0.4	0.5	0.4	0.4	0.7	0.7	0.7	0.6	0.7	0.5
Th	b.d.	b.d.	b.d.	b.d.	b.d.	25	27	26	28	28	28	32	37	34	35	32	34
U	3	3	6	3	2	6.7	7.7	7.5	8.1	8.0	8.1	12.0	12.3	12.1	11.3	11.3	11.5
Cl	64	52	143	218	64	194	b.d.	731	732	879	876	479	453	467	529	462	986
F	346	244	10	945	861	209	b.d.	272	146	421	569	968	452	537	445	464	226
T_{Zr} (C°)						795	763	782	762	758	762	743	741	743	742	742	745
$(La/Yb)_N$	2.6	2.6	3.4	6.5	9.6	6.5	7.0	7.6	5.2	6.7	6.5	1.6	1.6	1.1	2.7	1.9	1.8

Major elements in wt%, normalized to 100% anhydrous, trace elements in ppm

T_{Zr} zircon saturation temperature, *b.d.* below detection

data, including some rare earth elements (La, Ce, Nd, Sm, Eu, Yb, Lu), obtained from the Acigöl volcanics are summarised in Table 1. All rocks are calc-alkaline high-silica rhyolites (eastern group 74–76 wt% SiO_2, western group ~77 wt% SiO_2) and show geochemical features of volcanic arc magmas in tectonic discrimination diagrams after Pearce et al. (1984) (not shown). Within each group, little chemical variation exists (Fig. 3). An exception is Kocadag lava which contains higher abundances of compatible trace elements and less SiO_2 (73.6 wt%) compared to the other eastern group lavas. Overall, the compositional homogeneity implies a lack of compositional gradients in the magma chamber(s). We also note elevated halogen concentrations, with fluorine and chlorine abundances between

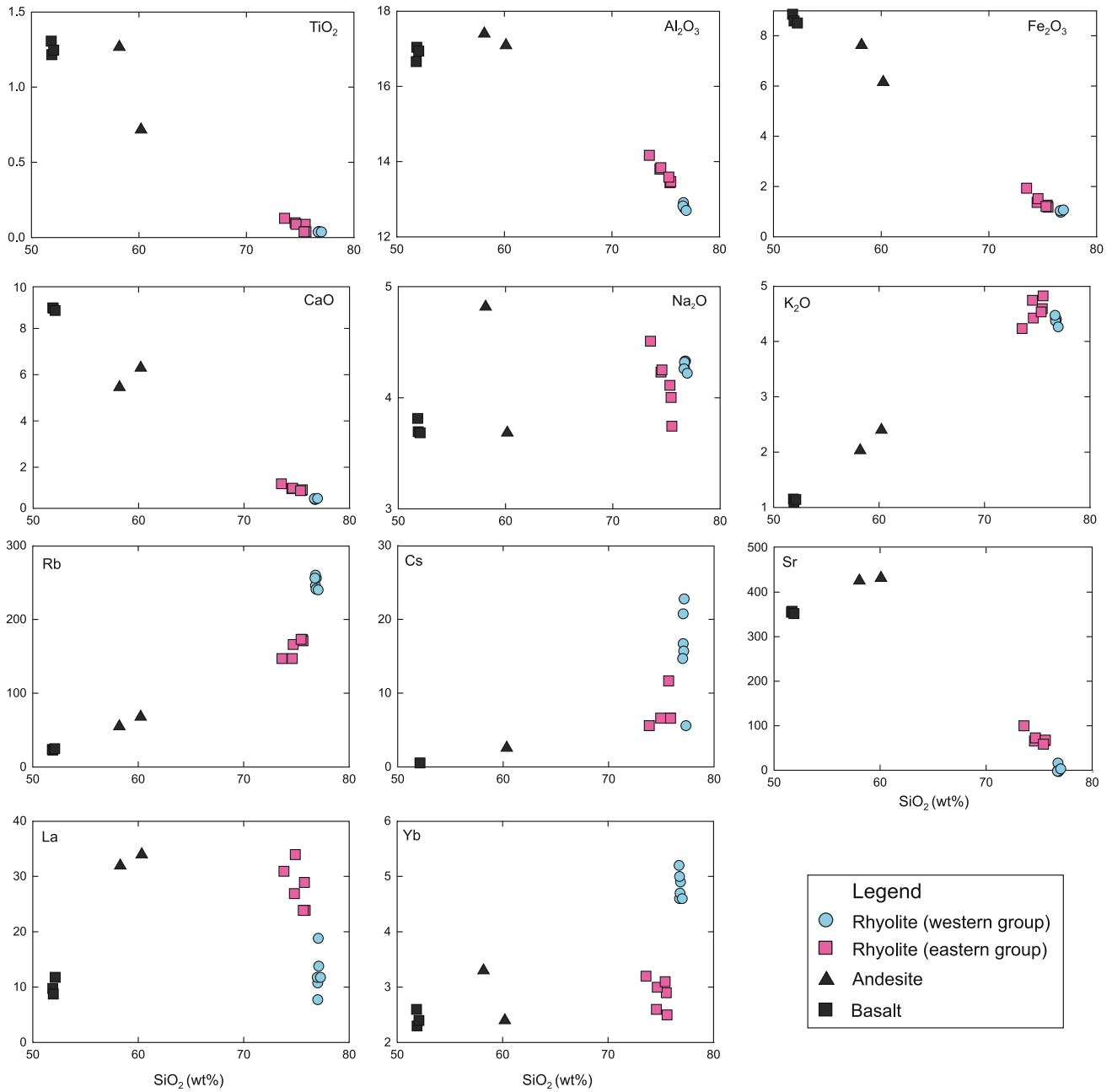

Fig. 3 Harker diagrams showing variations of major element oxides (wt%) and trace elements (ppm) for Acigöl lavas

146–968 and 194–986 ppm, respectively. These values are higher than those of felsic intrusive rocks (300–515 and 50–180 ppm, respectively), which have not experienced volcanic degassing (Gao et al. 1998).

There are, however, significant compositional differences between the two rhyolite groups. Particularly, the western group rhyolites (with Late Pleistocene eruption ages) are more enriched in incompatible trace elements and depleted in compatible elements than those of the eastern (Middle Pleistocene) precursors (Fig. 3). They have lower abundances of TiO_2, Al_2O_3, Fe_2O_3, MgO, CaO, P_2O_5, Sr, Ba, Zr, Ni, Cr and light rare earth element (LREE, represented by La, Ce and Nd) compared to the eastern group lavas. An opposite (i.e. increasing) trend in concentration can be found for SiO_2, MnO, Na_2O, Rb, Nb, Y, Cs, Th, U and F as well as for the heavy rare earth elements (HREE, represented by Yb and Lu). The western group rhyolite lava domes are, with one exception, extremely depleted in Sr (1–7 ppm, Güneydag = 20 ppm) and Ba (24–8 ppm, Güneydag = 524 ppm). These low trace element abundances require extensive fractional crystallization of feldspar-rich assemblages.

Based on the observed element distribution pattern, the chemical evolution of the rhyolites could be governed by dominant crystal/liquid fractionation processes of feldspar, biotite, quartz and FeTi oxides, with apatite and zircon as accessory phases, leading to residual high-silica liquids.

Zircon saturation temperatures were calculated from whole-rock geochemical data by using the experimental model of Watson and Harrison (1983). Whole-rock data are expected to yield a good approximation for magmatic Zr abundances because xenocrystic zircon is scarce (Schmitt et al. this issue), and the rocks are almost entirely aphyric. Zircon saturation temperatures for the eastern lavas are 795–762°C, whereas those for the younger domes are lower (745–741°C; Table 1).

There are additional geochemical indicators for an important role of accessory mineral fractionation in producing the geochemical characteristics of the Acigöl high-silica rhyolites. Western group high-silica rhyolites have significantly lower La/Yb compared to eastern group rhyolites (Table 1), possibly owing to the compatibility of LREE in accessory minerals such as monazite, allanite or chevkinite. Characteristic differences also exist between the high field strength elements Th and U: Th/U is close to the average terrestrial value (3.9 ± 0.1) in eastern group rhyolites (3.5–3.7), whereas lower values (2.7–3.1) are found in the western group rhyolites. This reflects preferential enrichment of the residual melt in uranium, possibly due to monazite, allanite or chevkinite fractionation although we could not clearly identify these minerals in our samples.

Reconnaissance sampling of mafic lavas from the Acigöl complex indicates two major compositional groups. Alacaşar and Karniyarik lavas are calc-alkaline basalts (in the NW part of the complex), whereas those from the Armutlu Tepe cinder cone (in the SE) are of andesite and trachyandesite composition.

Sr–Nd–Pb whole-rock isotope composition

Prior to this study, no isotope data have been published for Acigöl rocks. All isotope ratios are given in Table 2 and are depicted in Fig. 4. $^{87}Sr/^{86}Sr$ ratios in eastern group lavas range from 0.7059–0.7064. In comparison, $^{87}Sr/^{86}Sr$ of the western group domes are elevated (0.7065–0.7091), but lack any internal systematic variation by location. The basaltic lavas exposed in the north of the Acigöl field have low $^{87}Sr/^{86}Sr$ of 0.7040–0.7041, whereas the two transitional andesites from Armutlu Tepe cinder cone show intermediate values of 0.7053 (Fig. 4).

$^{143}Nd/^{144}Nd$ ratios of the eastern and western group lavas range from 0.51257–0.51265 (εNd from −1.4 to +0.2), and the rocks show virtually no difference in Pb isotope composition ($^{206}Pb/^{204}Pb$ = 18.87–18.88, $^{207}Pb/^{204}Pb$ = 15.65–15.67 and $^{208}Pb/^{204}Pb$ = 38.94–38.98). The average εNd value of the western group rhyolites is slightly higher (−0.2 ± 0.3; 2σ; $n = 6$) as compared to the eastern group lavas (−0.6 ± 0.4; $n = 6$). The εNd values of the basalts (2.8–3.6) are comparable with that of PREMA (prevalent

Table 2 Sr, Nd and Pb isotope composition of whole-rock samples from the Acigöl volcanic field and two granite samples outside the field

Sample	Rock type	$^{87}Sr/^{86}Sr$	±2σ	$^{143}Nd/^{144}Nd$	±2σ	εNd	T_{DM} (Ga)	$^{206}Pb/^{204}Pb$	$^{207}Pb/^{204}Pb$	$^{208}Pb/^{204}Pb$
KAR-1	Rhyolite (II)	0.708185	10	0.512643	9	0.1	0.81	18.882	15.666	38.990
KAL	Rhyolite (II)	0.707443	10	0.512606	8	−0.6	0.87	18.875	15.656	38.961
GÜN	Rhyolite (II)	0.709080	10	0.512632	10	−0.1	0.83	18.875	15.657	38.966
KUZ	Rhyolite (II)	0.706759	10	0.512606	10	−0.6	0.87	18.875	15.656	38.957
KOR	Rhyolite (II)	0.706996	10	0.512647	9	0.2	0.81	18.875	15.656	38.962
TEP	Rhyolite (II)	0.706494	10	0.512630	8	−0.2	0.83	18.876	15.657	38.966
BOG-1	Rhyolite (I)	0.706242	10	0.512622	10	−0.3	0.85	18.876	15.658	38.958
UAT	Pumice (I)	0.706335	10	0.512615	8	−0.4	0.86	18.879	15.660	38.963
TAS	Rhyolite (I)	0.706078	10	0.512586	10	−1.0	0.90	18.877	15.657	38.958
LAT	Pumice (I)	0.706440	9	0.512568	18	−1.4	0.93	18.874	15.656	38.950
ALA-4	Pumice (I)	0.706157	8	0.512617	10	−0.4	0.85	18.870	15.651	38.941
KOC	Rhyolite (I)	0.705891	10	0.512621	10	−0.3	0.85	18.884	15.663	38.981
ARM-2	Andesite	0.705325	10	0.512586	10	−1.0	0.90	18.866	15.647	38.939
ARM-1	Andesite	0.705284	7	0.512602	10	−0.7	0.88	18.859	15.655	38.973
ALA-2	Basalt	0.703954	9	0.512783	12	2.8	0.59	18.854	15.646	38.900
ALA-1	Basalt	0.703954	9	0.512780	10	2.8	0.59	18.851	15.649	38.903
KAR-2	Basalt	0.704107	9	0.512825	9	3.6	0.52	18.856	15.648	38.911
Tat-1	Granite	0.705168	10	0.512970	8	6.5	0.29	18.735	15.637	38.781
Tat-2	Granite	0.704565	8	0.512996	10	7.0	0.25	18.781	15.614	38.741

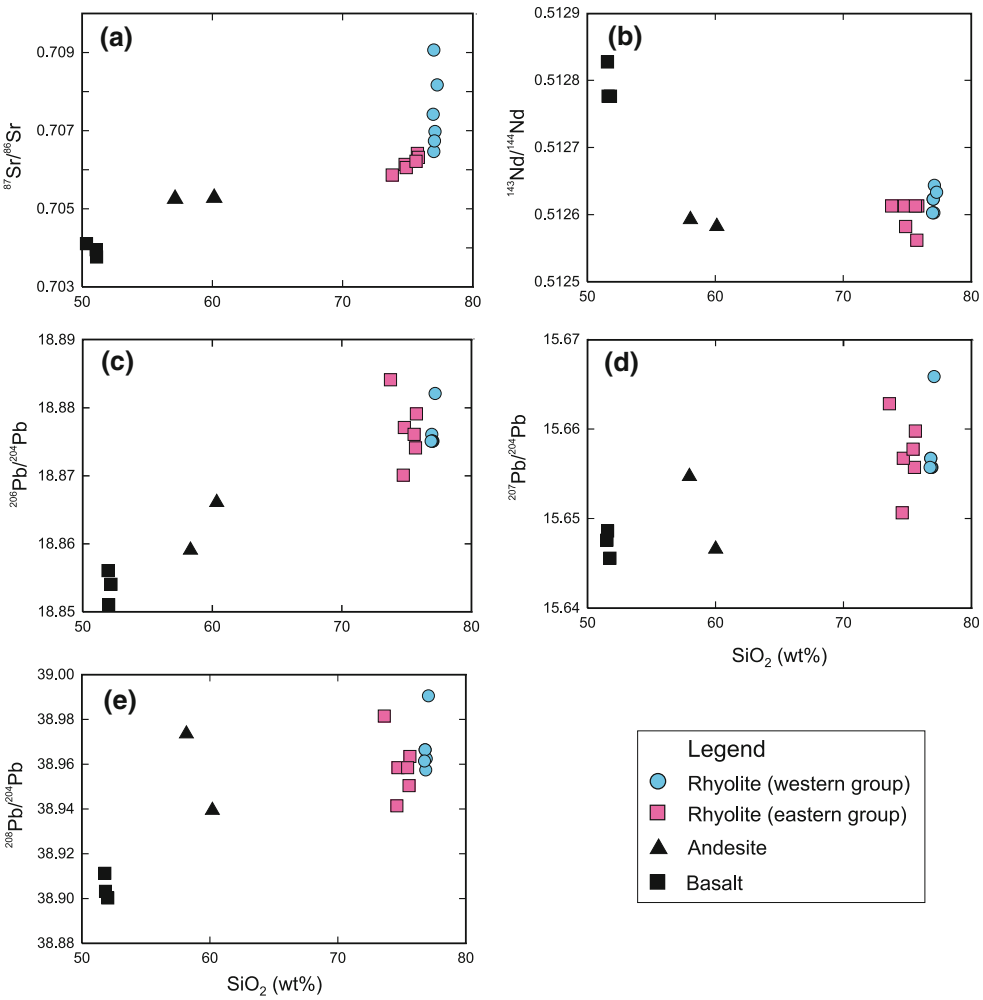

Fig. 4 Isotope composition of (**a**) $^{87}Sr/^{86}Sr$, (**b**) $^{143}Nd/^{144}Nd$, (**c**) $^{206}Pb/^{204}Pb$, (**d**) $^{207}Pb/^{204}Pb$ and (**e**) $^{208}Pb/^{204}Pb$ versus silica

mantle), whereas εNd values of the andesites are weakly sub-chondritic (−0.7 and −1.0) and overlap those of the rhyolites. Pb isotope ratios slightly increase from basalt to andesite and are $^{206}Pb/^{204}Pb$ = 18.85–18.87, $^{207}Pb/^{204}Pb$ = 15.646–15.655 and $^{208}Pb/^{204}Pb$ = 38.90–38.97 (Fig. 4). Pb concentrations in rhyolites are high compared to the basalts, reaching crustal values. But since most minerals crystallizing from mafic melts have very low crystal/liquid distribution coefficients for Pb, this element would become enriched during fractional crystallization from basalt to rhyolite.

We also present isotopic data for two granites west of the Acigöl volcanic field as a potential crustal component. Their present-day Sr–Nd–Pb isotopic composition (Table 2) is very distinct from other regional granitoids and represent some of the highest values (present-day $^{143}Nd/^{144}Nd$ = 0.51297–0.51300, or εNd = +6.5 to +7.0) measured for the CACC. This argues against any significant contribution from such rocks to the generation of the Acigöl rhyolites. A possible explanation is that these granites are silicic differentiates of Neotethyan ocean crust. For example, plagiogranites, interspersed with mafic rocks, are commonly present in ophiolite fragments within the CACC (Floyd et al. 1998, 2000).

Zircon oxygen data

The $\delta^{18}O$(zircon) averages are indistinguishable for eastern domes Bogazköy (6.2 ± 0.2‰; 2σ; MSWD = 1.4; n = 9) and Taşkesik (6.2 ± 0.3‰; MSWD = 1.5; n = 11). Sample KOC from the compositionally distinct eastern Kocadag dome yields similar $\delta^{18}O$(zircon) = 5.9 ± 0.2‰ (MSWD = 1.6; n = 12). Zircons from western group domes are slightly lower in $\delta^{18}O$ (average 5.7 ± 0.2‰; MSWD = 1.2; n = 21; Table 3; Fig. 5). The lowest value of 5.3 ± 0.5‰ was found for zircon from an ejecta clast in Acigöl maar deposits that represent the youngest rhyolitic volcanic activity at Acigöl. Two zircon xenocryts dated at ~73 and ~9 Ma (Schmitt et al. this volume) have distinctively higher $\delta^{18}O$ values of 8.9 and 8.2‰, respectively. A negative correlation exists between $\delta^{18}O$(zircon) and εNd values consistent with lower degrees of crustal

Table 3 Oxygen isotope ratios of zircons from the Acigöl volcanic field

Sample	Locality	Rock type	$\delta^{18}O$ (‰)	$\pm 2\sigma$	N
TEP	Tepeköy	Rhyolite II	5.46	0.20	4
KUZ	Kuzey	Rhyolite II	5.85	0.16	13
KAR-1	Karniyarik	Rhyolite II	5.42	0.31	4
ACI	Acigöl maar	Rhyolite II	5.25	0.45	9
BOG-1	Bogazköy	Rhyolite I	6.17	0.24	9
KOC	Kocadag	Rhyolite I	6.02	0.26	13
TAS	Taşkesik	Rhyolite I	6.19	0.22	11

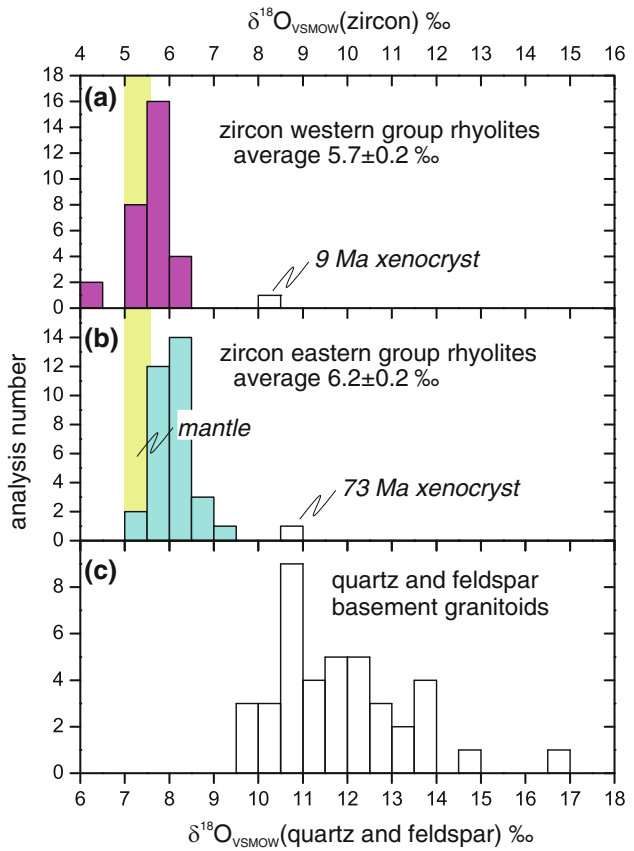

Fig. 5 Histograms of $\delta^{18}O$(zircon) for lavas from eastern group (**a**) and western group (**b**) rhyolites. Grey columns indicate average $\delta^{18}O$ of mantle zircons; (**c**) $\delta^{18}O$(quartz/feldspar) data for felsic central Anatolian granitoids (Boztug and Arehart 2007)

contamination in younger rhyolites, but an inverse correlation between $\delta^{18}O$(zircon) and $^{87}Sr/^{86}Sr$, as would be expected in such scenario, does not exist (Fig. 6). As will be discussed later, addition of exogenous Sr may account for this finding.

In felsic igneous rocks ($\sim$75 wt% SiO_2), $\delta^{18}O$ values in zircons are estimated to be 2.1‰ lower compared to the corresponding whole-rock value (e.g. Trail et al. 2009). The $\delta^{18}O$(zircon) values of Acigöl rhyolites (i.e. eastern group = 6.2 ± 0.2‰, western group = 5.7 ± 0.2‰) are far too low for zircon crystallizing from anatectic regional basement rocks (Fig. 5). On the other hand, the 2–3‰ difference between rhyolite zircons and zircon xenocrysts indicates the presence of similar basement rocks underneath Acigöl. Zircons in western group rhyolites are almost indistinguishable from those crystallizing from direct mantle derivates (5.3 ± 0.3‰) (Valley et al. 1998).

Discussion

$^{87}Sr/^{86}Sr$ shift in western group rhyolites: assimilation or post-magmatic alteration?

Sr isotope ratios of Acigöl volcanics appear more radiogenic compared to Miocene ignimbrites of the CVP (Fig. 7). However, Acigöl rhyolites, in particular those of the western group, have very low Sr abundances (generally <7 ppm). The $^{87}Sr/^{86}Sr$ ratios do not correlate with chemical parameters such as Rb/Sr or Sr abundances indicating that Sr isotopic composition is decoupled from the degree of differentiation of the rhyolites. The overall depletion of Sr (as well as Ba) in the western group rhyolites is a result of extensive feldspar fractionation. In other cases, similar variations in Sr ratios among Sr-poor high-silica rhyolites have been attributed to pre-eruptive in situ decay of ^{87}Rb (Mahood and Halliday 1988). However, the absence of a correlation between Rb/Sr, Sr concentration and $^{87}Sr/^{86}Sr$ is inconsistent with in situ radiogenic Sr ingrowth over time as an explanation for the isotopic variability of the Acigöl rhyolites. Another reason for ruling this out is the unrealistically long time span required to generate $^{87}Sr/^{86}Sr$ differences—a minimum of hundreds of thousands of years, and for most of these samples, much longer. Low Sr abundances make these rocks very vulnerable to assimilation of high-$^{87}Sr/^{86}Sr$ country rocks. Because angular granitic clasts are present (at <0.5 mm diameter too small to be separated from the crushed rock), we urge caution in interpreting elevated Sr isotopic compositions to reflect magmatic assimilation. The presence of unmelted granitic xenoliths (Fig. 2c) and incompletely degassed zircon crystals (Schmitt et al. this volume) is evidence that country-rock contamination occurred late, most likely during the eruption. Moreover, there is geochemical evidence that alteration also affected the Sr isotopic composition of whole-rock samples. The $^{87}Sr/^{86}Sr$ isotope ratios versus LOI plot shows a strong positive correlation for low Sr western group rhyolites and a weak correlation for the eastern group (Fig. 8). This strongly suggests the addition of extrinsic radiogenic Sr via alteration, which is more obvious if Sr abundances in the rocks are low. Infiltration of Sr and an increase in $^{87}Sr/^{86}Sr$ ratios may result from contact with rainwater or possibly

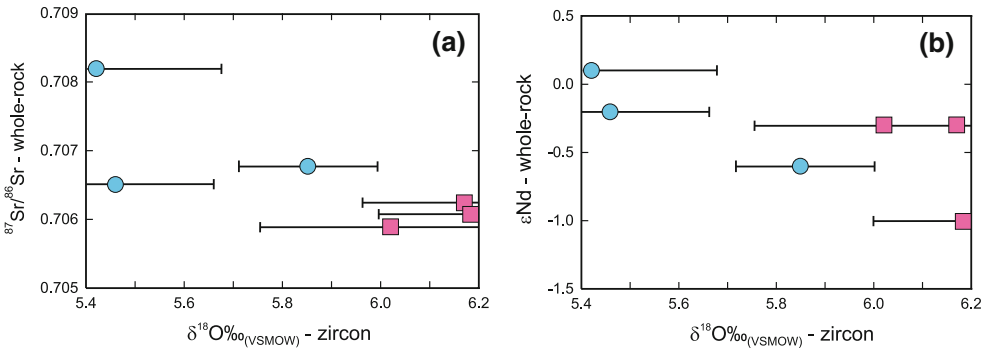

Fig. 6 **a** $^{87}Sr/^{86}Sr$ and **b** εNd values versus $\delta^{18}O$(zircon) data. Errors are shown for $\delta^{18}O$(zircon) data and are smaller than symbols for Sr and Nd. Squares = eastern group rhyolites, circles = western group rhyolites

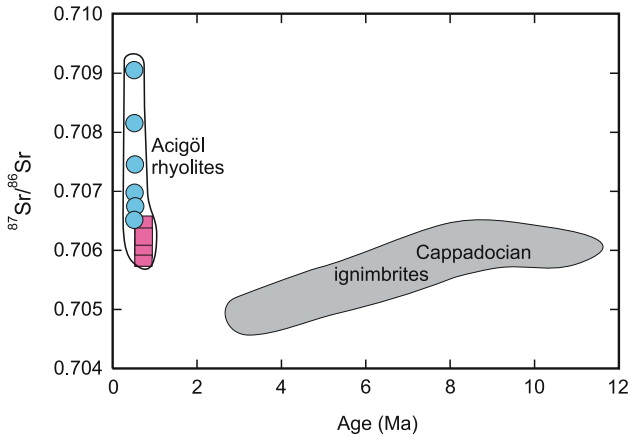

Fig. 7 $^{87}Sr/^{86}Sr$ isotope ratios for Miocene ignimbrites (Temel et al. 1998) versus age. Eastern and western group rhyolites from the Acigöl field are shown for comparison. Symbols as in Fig. 6

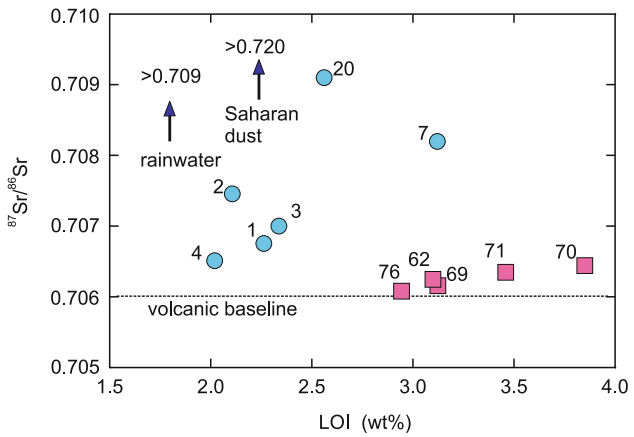

Fig. 8 LOI (loss on ignition) versus $^{87}Sr/^{86}Sr$ isotope ratios for eastern and western group rhyolites. Numbers next to symbols denote Sr content (in ppm). Sr isotope ratios for rainwater close to that of marine Sr (Bacon and Bain 1995) and average Saharan dust (Ehrmann et al. 2007) are indicated for comparison. 'Volcanic baseline composition' indicates location of a hypothetically uncontaminated and unaltered rhyolitic lava system. Symbols as in Fig. 6

contamination by exogenous dust particles (Stewart et al. 2001). Cappadocian Quaternary volcanics are frequently capped by wind-blown silts from adjacent plains west of Acigöl and calcrete layers (Türkecan et al. 2004). Radiogenic Sr washed out from such materials and added to the rhyolites during hydration could explain the elevated Sr isotope ratios in the rhyolites. The slight positive trend between Sr isotopic ratios and LOI for the eastern group lavas (Fig. 8) suggests that these too have been affected by post-magmatic Sr addition, but the effects of country rock contamination and alteration are mitigated owing to their higher Sr abundances (62–103 ppm).

Relationship between sequentially erupted rhyolites

The age progression from less to more evolved silicic magmas in the Acigöl rhyolite field raises questions about a potential genetic link between both suites. The eastern and western rhyolite groups are chemically distinct, with no evidence for significant compositional variation within each group. This implies a relatively homogeneous magma reservoir or lack of a compositionally zoned magmatic system for each eruption group. There is also a temporal trend of decreasing zircon saturation temperatures (from 762–795 to 741–745°C), suggestive of a direct genetic lineage between the two suites via cooling and crystal fractionation. Zircon $\delta^{18}O$ isotope ratios, however, show subtle differences between the two silicic groups, implying that the western group rhyolites cannot be derived from the eastern group by direct fractional crystallization. The variability in zircon oxygen isotope composition requires a smaller contribution of crustal material in the western group rhyolites compared with their older counterparts erupted in the eastern part of the Acigöl complex. This isotopic distinction also holds for εNd between the two rhyolite groups (Fig. 6). The clear spatial segregation (older group in east, younger group in west) supports eruption from separate magma reservoirs. This is consistent with a lack of zircon antecrysts of Middle Pleistocene age

in the subsequently erupted western rhyolites (Schmitt et al. this volume).

Origin of rhyolites and their relationship to basalt

An origin of the Acigöl rhyolites by crustal melting of the metamorphic basement is precluded because the δ^{18}O(zircon) values for the younger rhyolite domes are in the range of mantle values and their Nd isotope ratios are close to chondritic composition. In addition, the rhyolites have Sr isotopic composition different from the basement rocks of the region (Köksal and Göncüoğlu 2008, and references therein) albeit the Sr isotopes are more variable due to late-stage contamination and alteration. Anatolian granitoids have present-day $^{87}Sr/^{86}Sr$ ratios mainly in the range between 0.706–0.722 and εNd values between −3 and −9 (see data compilation in Köksal and Göncüoğlu 2008). Crustal basement rocks are thus far too evolved in their isotopic composition to represent the source of the rhyolites. The exceptions are plagiogranites in ophiolitic nappe sequences with strongly positive εNd and low $^{87}Sr/^{86}Sr$ (Table 2), but these compositions are also distinct from those of the rhyolites. Oxygen isotopes in zircon xenocrysts are consistent with high quartz and feldspar δ^{18}O values for CCVC granitoids (Fig. 5; Boztug and Arehart 2007).

By contrast, the εNd values for the Acigöl rhyolites overlap within error with those of the andesites (εNd between 0 and −1). The highly evolved geochemical composition along with primitive Nd isotope composition and low zircon δ^{18}O values (5.7–6.2‰) are also consistent with an origin by fractional crystallization from a mafic melt. The origin of Upper Miocene to Quaternary ignimbrites from Cappadocia was related to sources dominated by mantle material (Temel et al. 1998). A decrease in Sr isotopic ratio from ~0.7060 to ~0.7046 through time (i.e. from 13–2 Ma, Fig. 7) suggests increasing mantle contributions (Temel et al. 1998). The basalts from the Acigöl field have $^{87}Sr/^{86}Sr$ ratios around 0.7040–0.7041, close to the Sr isotope composition of the most primitive ignimbrite investigated by Temel et al. (1998). Therefore, at least some felsic ignimbrites in the CVP are apparently mantle-derived.

The Acigöl rhyolites are ~3 εNd units lower than Nd of regional basalts, whereas oxygen isotopes (correcting for a +2‰ fractionation between melt and zircon at 700°C; Trail et al. 2009) are elevated by at most +2‰ δ^{18}O units relative to mantle basalt (Eiler 2001). A direct derivation of the rhyolites from the mantle is therefore unlikely although fractionation of mafic minerals from basalt will result in slightly higher (+0.7‰) δ^{18}O of the residual melt (Eiler 2001). Instead, the slightly elevated δ^{18}O values estimated for the rhyolite melts suggest some contamination within the crust. Elevated Sr isotopic compositions would also point to a crustal contaminant with $^{87}Sr/^{86}Sr$ of >0.7091, consistent with literature data for widely distributed central Anatolian basement rocks (Köksal and Göncüoğlu 2008). Open-system processes, however, such as magma mixing or crustal assimilation cannot be a priori distinguished from contamination during eruption and alteration from Sr isotope systematics alone.

The crustal component in the Acigöl rhyolites is probably best represented by CVCC granitoids (Boztug and Arehart 2007; Köksal and Göncüoğlu 2008), for which Cretaceous zircon xenocrysts provide direct evidence that similar rocks are present underneath the Acigöl complex (Schmitt et al. this volume). Because the Armutlu Tepe andesites are isotopically intermediate between the basalts and the rhyolites, they also appear to have interacted with crustal rocks. Thus, possible scenarios for rhyolite petrogenesis are (1) derivation from basaltic mantle melts affected by crustal assimilation or (2) derivation from hybrid magma sources produced by partial melting of mainly mantle and minor crustal components. Hereafter, we briefly discuss both scenarios.

As a general tendency, Sr–Nd–Pb isotopic differences between basalts and rhyolites from the Acigöl volcanic field are smaller than between rhyolites and central Anatolian basement crust. These isotope ratios likely record the effect that the rocks have undergone only minor crustal contamination, whereas high SiO_2, low Ba and Sr especially in the western group rhyolites, requires strong amount of shallow crustal fractionation. In order to estimate the amount of crust material contributing to rhyolite generation, we first consider the case where rhyolite formed from a parental basaltic or andesitic liquid via assimilation fractional crystallization (AFC, DePaolo 1981). Mass balance parameters and end members in AFC models are generally non-unique, but, nevertheless, permit first-order assessments about the relative amounts of mantle versus crustal materials involved. For a range of regional basalt parents and crustal assimilants (isotopic compositions and concentrations for mafic end member from Tables 1 and 2 and for basement rocks from Köksal and Göncüoğlu 2008), AFC models indicate a maximum of ~10% crustal component with $^{87}Sr/^{86}Sr = 0.710–0.715$ and $^{143}Nd/^{144}Nd = 0.5122–0.5123$ in Acigöl rhyolites. This model could also explain the minor isotopic and trace element differences between western and eastern rhyolite groups, for example if slightly different r values (mass assimilation rate compared to the degree of fractional crystallization) in the range of 0.10–0.15 were operating or if different parental magmas (basalt, andesite) were involved. The extremely low Sr abundances of the western group rhyolites (<7ppm), however, cannot be satisfactorily reproduced by AFC for Sr concentration of average upper

continental crust (320 ppm, Rudnick and Gao 2003) and require a two-stage evolution with late-stage fractional crystallization. Partial melting of an isotopically hybrid source dominated by a mantle component that subsequently undergoes fractionation at shallower levels would be a feasible scenario to explain all major compositional (particularly the high-silica and low Sr and Ba contents) and isotopic features. Such hybrid melts could have been pre-formed within a deep crustal hot zone (Annen et al. 2006) where melting of hybrid rocks (i.e. melts produced by mixing of residual basaltic melts and crustal partial melts) and melt segregation was decoupled from subsequent fractionation processes in middle to upper crustal levels.

Conclusions

The Acigöl volcanic field evolved through two major eruption cycles of high-silica rhyolites. Geochemical and isotopic differences are very minor within each eruptive cycle, but pronounced between the temporally and spatially distinct Middle Pleistocene (eastern) and Late Pleistocene (western) groups. Isotopic compositions of the rhyolites generally fall between values for associated basalts/andesites and regional granitic basement rocks. Despite trace element and major element trends that suggest more differentiated magma compositions erupting later in the evolution of the complex, the two rhyolite groups are isotopically distinct, precluding a closed-system differentiation model. Instead, isotope and trace elemental compositions of the rhyolites are linked to those of coeval basalts and andesites via separate evolutionary paths involving derivation from a hybrid magma source and/or multi-stage fractional crystallization and minor (<10%) rates of crustal contamination. The younger rhyolites erupted as more differentiated magmas, whereas the older rhyolites show evidence for slightly stronger contamination with crustal materials. This also suggests that a higher volume fraction of crustal material is associated with the larger eruption volumes in the Middle Pleistocene, whereas the magma system that fed Late Pleistocene small-volume rhyolite eruptions may not have been sufficiently large to undergo significant wall-rock assimilation or mixing. We also emphasise that contamination and/or alteration mask these trends for low Sr, high-silica rhyolites. Thus, petrogenetic modelling of high-silica suites should be based on robust geochemical and isotopic indicators, and high-spatial resolution analysis of zircon is an excellent way of accomplishing this. High-silica rhyolites at Acigöl evolved independently from each other arguing against the presence of a long-lived shallow crustal magma reservoir underneath the complex.

Acknowledgments We acknowledge the help of S. Eroglu, S. Jahn, E. Reitter and H. Taubald during geochemical and isotope analyses. Janet C. Harvey is thanked for assistance in the field and Erkan Aydar for helpful discussions about Cappadocian volcanism. Comments and suggestions by Calvin Miller and Jonathan Miller have helped us to improve the quality of the manuscript. Jochen Hoefs is thanked for editorial handling. This study was supported by a grant from the German Science Foundation (Si 718/9-1). The ion microprobe facility at UCLA is partly supported by a grant from the Instrumentation and Facilities Program, Division of Earth Sciences, National Science Foundation.

References

Alıcı-Şen P, Temel T, Gourgaud A (2004) Petrogenetic modelling of Quaternary post-collisional volcanism: a case study of central and eastern Anatolia. Geol Mag 141:81–98

Annen C, Blundy JD, Sparks RSJ (2006) The genesis of intermediate and silicic magmas in deep crustal hot zones. J Petrol 47:505–539

Aydin F (2008) Contrasting complexities in the evolution of calc-alkaline and alkaline melts of the Nigde volcanic rocks, Turkey: textural, mineral chemical and geochemical evidence. Eur J Mineral 20:101–118

Bachmann O, Bergantz GW (2004) On the origin of crystal-poor rhyolites: extracted from batholithic crystal mushes. J Petrol 45:1565–1582

Bacon JR, Bain DC (1995) Characterization of environmental water samples using strontium and lead stable isotope compositions. Environ Geochem Health 17:39–49

Batum I (1978) Geology and petrography of Acıgöl and Göllüdağ volcanics at southwest of Nevşehir central Anatolia, Turkey. Yerbilimleri 4:50–69 (in Turkish with English abstract)

Beekman PH (1966) The Pliocene and Quaternary volcanism in the Hasan Dag-Melendiz Dag region. Bull Miner Res Explor Inst Turk 66:90–105 (in Turkish)

Bigazzi G, Yegingil Z, Ercan T, Oddone M, Ozdogan M (1993) Fission-track dating obsidians in central and northern Anatolia. Bull Volcanol 55:588–595

Bozkurt E (2001) Neotectonics of Turkey—a synthesis. Geodin Acta 14:3–30

Boztug D, Arehart GB (2007) Oxygen and sulfur isotope geochemistry revealing a significant crustal signature in the genesis of the post-collisional granitoids in central Anatolia, Turkey. J Asian Earth Sci 30:403–416

Chataigner C, Poidevin JL, Arnaud NO (1998) Turkish occurrences of obsidian and use by prehistoric peoples in the Near East from 14, 000 to 6000 BP. J Volcanol Geotherm Res 85:517–537

Christiansen RL (2001) The Quaternary and Pliocene Yellowstone plateau volcanic field of Wyoming, Idaho, and Montana. US Geol Surf Prof Pap 729-G:120 pp

Cousens BL, Henry CD, Harvey BJ, Brownrigg T, Prytulak J, Allan JF (2011) Secular variations in magmatism during a continental arc to post-arc transition: Plio-Pleistocene volcanism in the Lake Tahoe/Truckee area, Northern Sierra Nevada, California. Lithos 123:225–242

Deniel C, Aydar E, Gourgaud A (1998) The Hasan Dagi stratovolcano (central Anatolia, Turkey): evolution from calc-alkaline to alkaline magmatism in a collision zone. J Volcanol Geotherm Res 87:275–302

DePaolo DJ (1981) Trace element and isotopic effects of combined wallrock assimilation and fractional crystallization. Earth Planet Sci Lett 53:189–202

Dewey JF, Hempton MR, Kidd WSF, Saroglu F, Şengör AMC (1986) Shortening of continental lithosphere: the neotectonics of

Eastern Anatolia—a young collision zone. Geol Soc Lond Spec Publ 19:1–36

Dilek Y, Sandvol E (2009) Seismic structure, crustal architecture and tectonic evolution of the Anatolian-African plate boundary and the Cenozoic orogenic belts in the Eastern Mediterranean region. Geol Soc Lond Spec Publ 327:127–160

Dirik K, Göncüoğlu C (1996) Neotectonic characteristics of central Anatolia. Int Geol Rev 38:807–817

Druitt TH, Brenchley PJ, Gökten YE, Francaviglia V (1995) Late Quaternary rhyolitic eruptions from the Acigöl complex, central Turkey. J Geol Soc Lond 152:655–667

Ehrmann W, Schmiedl G, Hamann Y, Kuhnt T, Hemleben C, Siebel W (2007) Clay minerals in late glacial and Holocene sediments of the northern and southern Aegean Sea. Palaeogeogr Palaeoclimatol Palaeoecol 249:36–57

Eiler JM (2001) Oxygen isotope variations of basaltic lavas and upper mantle rocks. In: Valley JW, Cole DR (eds) Stable isotope geochemistry. Rev Miner 43:319–364

England A, Eastwood WJ, Roberts CN, Turner R, Haldon JF (2008) Historical landscape change in Cappadocia (central Turkey): a palaeoecological investigation of annually laminated sediments from Nar lake. Holocene 18:1229–1245

Faccenna C, Bellier O, Martinod J, Piromallo C, Regard V (2006) Slab detachment beneath eastern Anatolia: a possible cause for the formation of the North Anatolian fault. Earth Planet Sci Lett 242:85–97

Floyd PA, Yaliniz MK, Göncüoglu MC (1998) Geochemistry and petrogenesis of intrusive an extrusive ophiolitic plagiogranites, Central Anatolian Crystalline Complex, Turkey. Lithos 42: 225–241

Floyd PA, Göncüoglu MC, Winchester JA, Yaliniz MK (2000) Geochemical character and tectonic environment of Neotethyan ophiolitic fragments and metabasites in the Central Anatolian Crystalline Complex, Turkey. In: Bozkurt E, Winchester JA, Piper JDA (eds) Tectonics and magmatism in Turkey and the surrounding area. Geol Soc Lond Spec Publ 173:183–202

Gao S, Luo TC, Zang BR, Zang HF, Han YW, Hu YK, Zhao ZD (1998) Chemical composition of the continental crust as revealed by studies in east China. Geochim Cosmochim Acta 62:1959–1975

Glazner AF, Coleman DS, Bartley JM (2008) The tenuous connection between high-silica rhyolites and granodiorite plutons. Geology 36:1047–1050

Goldstein SJ, Murrell MT, Janecky DR (1989) Th and U isotopic systematics of basalts from the Juan de Fuca and Gorda Ridges by mass spectrometry. Earth Planet Sci Lett 96:134–146

Göncüoğlu MC (1986) Geochronological data from the southern part (Niğde area) of the central Anatolian massif. Bull Miner Res Explor Inst Turk 105(106):83–96

Göncüoğlu MC, Toprak V (1992) Neogene and quaternary volcanism of central Anatolia: a volcano-structural evaluation. Bull Sec Volcanol Soc Géol France 26:1–6

Innocenti F, Mazzuoli R, Pasquaré G, Radicati di Brozolo F, Villari L (1975) The Neogene calcalkaline volcanism of central Anatolia: geochronological data on Kayseri-Nigde area. Geol Mag 112: 349–360

Jiménez-Munt I, Sabadini R, Gardi A, Bianco G (2003) Active deformation in the Mediterranean from Gibraltar to Anatolia inferred from numerical modeling and geodetic and seismological data. J Geophys Res 108(B1):2006

Jones S (2007) The Toba supervolcanic eruption: Tephra-fall deposits in India and paleoanthropological implications. In: Petraglia MD and Allchin B (eds) The evolution and history of human populations in South Asia. Springer, Dordrecht, pp 173–200

Koçyiğit A, Beyhan A (1998) A new intracontinental transcurrent structure: the central Anatolian fault zone, Turkey. Tectonophysics 284:317–336

Köksal S, Göncüoğlu MC (2008) Sr and Nd isotopic characteristics of some S-, I- and A-type granitoids from central Anatolia. Turkish J Earth Sci 17:111–127

Kürkçüoglu BES, Aydar E, Gourgaud A, Gündogdu N (1998) Geochemical approach to magmatic evolution of Mt. Erciyes stratovolcano central Anatolia, Turkey. J Volcanol Geotherm Res 85:473–494

Le Pennec JL, Bourdier JL, Froger JL, Temel A, Camus G, Gourgaud A (1994) Neogene ignimbrites of the Nevşehir plateau (central Turkey): stratigraphy, distribution and source constraints. J Volcanol Geotherm Res 63:59–87

Mahood GA, Halliday AN (1988) Generation of high-silica rhyolite—a Nd, Sr, and O isotopic study of Sierra-La-Primavera, Mexican Neovolcanic belt. Contrib Mineral Petrol 100:183–191

Metz JM, Mahood GA (1985) Precursors to the Bishop tuff eruption: Glass Mountain, Long Valley, California. J Volcanol Geotherm Res 90:11121–11126

Metz JM, Mahood GA (1991) Development of the Long Valley, California, magma chamber recorded in precaldera rhyolite lavas of Glass mountain. Contrib Mineral Petrol 106:379–397

Miller CF, Mittlefehldt DW (1984) Extreme fractionation in felsic magma chambers: a product of liquid-state diffusion or fractional crystallization? Earth Planet Sci Lett 68:151–158

Mouralis D, Pastre JF, Kuzucuoglu C, Türkecan A, Atici Y, Slimak L, Guillou H, Kunesch S (2002) Les complexes volcaniques rhyolitiques quaternaires d'Anatolie centrale (Göllü dag et Acigöl, Turquie): genèse, instabilité, contraintes environnementales. Quatenaire 13:219–228

Notsu K, Fujitani T, Ui T, Matsuda J, Ercan T (1995) Geochemical features of collision-related volcanic rocks in central and eastern Anatolia, Turkey. J Volcanol Geotherm Res 64:171–191

Olanca K (1994) Géochimie des laves quaternaires de Cappadoce (Turquie). Les appareils monogéniques. PhD thesis, Univ Clermont-Ferrand, 156 pp

Pasquarè G (1968) Geology of the Cenozoic volcanic area of central Anatolia. Atti Accademia Nazionale Lincei Memoire 9:54–204

Pasquarè G, Poli S, Vezzoli L, Zanchi A (1988) Continental arc volcanism and tectonic setting in central Anatolia, Turkey. Tectonophysics 146:217–230

Pearce JA, Harris NBW, Tindle AG (1984) Trace-element discrimination diagrams for the tectonic interpretation of granitic-rocks. J Petrol 25:956–983

Poupeau G, Le Bourdonnec FX, Carter T, Delerue S, Shackley MS, Barrat JA, Dubernet S, Moretto P, Calligaro T, Milić M, Kobayashi K (2010) The use of SEM-EDS, PIXE and EDXRF for obsidian provenance studies in the Near East: a case study from Neolithic Çatalhöyük (central Anatolia). J Archaeol Sci 37:2705–2720

Rampino MR, Self S (1992) Volcanic winter and accelerated glaciation following the Toba super-eruption. Nature 359:50–52

Robertson AHF (2000) Mesozoic-Tertiary tectonic-sedimentray evolution of a south Tethyan oceanic basin and its margins in southern Turkey. In: Bozkurt E, Winchester JA and Piper JDA (eds) Tectonics and magmatism in Turkey and the surrounding area. Geol Soc Lond Spec Publ 173:97–138

Rudnick RL, Gao S (2003) The composition of the continental crust. In: Rudnick RL (ed) The crust. Treatise on geochemistry, vol 3. Elsevier-Pergamon, Oxford, pp 1–64

Saunders KE, Morgan DJ, Baker JA, Wysoczanski RJ (2010) The magmatic evolution of the Whakamaru supereruption, New Zealand, constrained by a microanalytical study of plagioclase and quartz. J Petrol 51:2465–2488

Şengör AMC, Özeren MS, Keskin M, Sakinç M, Özbakır AD, Kayan I (2008) Eastern Turkish high plateau as a small Turkic-type orogen: implications for post collisional crust-forming processes in Turkic-type orogens. Earth Sci Rev 90:1–48

Serpelloni E, Vannucci G, Pondrelli S, Argnani A, Casula G, Anzidei M, Baldi P, Gasperini P (2007) Kinematics of the western Africa-Eurasia plate boundary from focal mechanisms and GPS data. Geophys J Int 169:1180–1200

Slimak L, Kuhn SL, Roche H, Mouralis D, Buitenhuis H, Balkan-Atli N, Binder D, Kuzucuoglu C, Guillou H (2008) Kaletepe Deresi 3 (Turkey): archaeological evidence for early human settlement in central Anatolia. J Hum Evol 54:99–111

Stephenson R, Marti Y, Okay A, Robertson AHF, Saintot A, Stovba S, Khriachtchevskaia O (2004) Transect VIII: Eastern European Craton—Crimea—Black Sea—Anatolia—Cyprus—Levant Sea—Red Sea. In: Cavvaza W, Roure F, Spakman W, Stampfli GM, Ziegler PA (eds) The TRANSMED Atlas—the Mediterranean region from crust to mantle. Springer, Berlin

Stewart BW, Capo RC, Chadwick OA (2001) Effects of rainfall on weathering rate, base cation provenance, and Sr isotope composition of Hawaiian soils. Geochim Cosmochim Acta 65:1087–1099

Streck MJ, Grunder AL (2008) Phenocryst-poor rhyolites of bimodal, tholeiitic provinces: the Rattlesnake tuff and implications for mush extraction models. Bull Volcanol 70:385–401

Temel A, Gündogdu MN, Gourgaud A, Le Pennec JL (1998) Ignimbrites of Cappadocia (central Anatolia, Turkey): petrology and geochemistry. J Volcanol Geotherm Res 85:447–471

Toprak V (1998) Vent distribution and its relation to regional tectonics, Cappadocian volcanics, Turkey. J Volcanol Geotherm Res 85:55–67

Trail D, Mojzsis SJ, Harrison TM, Schmitt AK, Watson EB, Young ED (2007) Constraints on Hadean zircon protoliths from oxygen isotopes, Ti-thermometry, and rare earth elements. Geochem Geophys Geosyst 8:22 pp

Trail D, Bindeman IN, Watson EB, Schmitt AK (2009) Experimental calibration of oxygen isotope fractionation between quartz and zircon. Geochim Cosmochim Acta 73:7110–7126

Tryon CA, Logan MAV, Mouralis D, Kuhn SL, Slimak L, Balkan-Atil N (2009) Building a tephrostratigraphic framework for the Paleolithic of central Anatolia, Turkey. J Archaeol Sci 36: 637–652

Türkecan A, Kuzucuoğlu C, Mouralis D, Pastre J-F, Atıcı Y, Guillou H, Fontugne M (2004) Upper Pleistocene volcanism and palaeogeography in Cappadocia, Turkey. MTA-CNRS-TÜBİ-TAK 2001-2003 Research Programme. Tübitak Project No. 101Y109, MTA Report No. 10652 (unpublished) 180 pp

Valley JW, Kinny PD, Schulze DJ, Spicuzza MJ (1998) Zircon megacrysts from kimberlite: oxygen isotope variability among mantle melts. Contrib Mineral Petrol 133:1–11

Viereck-Götte L, Lepetit P, Gürel A, Ganskow G, Çopuroğlu I, Abratis M (2010) Revised volcanostratigraphy of the Upper Miocene to Lower Priocene Ürgüp Formation, central Anatolian volcanic province, Turkey. Geol Soc Am Spec Pap 464:85–112

Watson EB, Harrison TM (1983) Zircon saturation revisited - temperature and composition effects in a variety of crustal magma types. Earth Planet Sci Lett 64:295–304

Yildirim T, Özgür R (1981) The Acigöl caldera. Jeomorfoloji Dergisi (Bulletin of Geomorphology) 10:59–70 (in Turkish)